Sādhanā (2026)51:198
https://doi.org/10.1007/s12046-026-03162-0

Delayed detached eddy simulations of heat transfer and flow over smooth and circumferentially grooved tandem circular cylinders

ENES OZTURK[1] and SEYFETTIN BAYRAKTAR[2,*]

[1]UZMAR Shipbuilding, 41090 Basiskele, Kocaeli, Turkey
[2]Department of Marine Engineering, Naval Architecture and Maritime Faculty, Yildiz Technical University, 34349 Istanbul, Turkey
*Corresponding Author.
E-mail: enes_ozturk41@hotmail.com; sbay@yildiz.edu.tr

MS received 1 September 2024; revised 5 September 2025; accepted 11 December 2025
© The Author(s), under exclusive licence to Indian Academy of Sciences 2026

Abstract. In the present study, two-dimensional transient flow over circular cross-sectional smooth and grooved cylinders in tandem is investigated comparatively using a delayed detached eddy simulation (DDES) based on the shear stress transport (SST) k-omega turbulence model for various Reynolds numbers ($10 \leq Re_D \leq 65\times10^3$). The flow and heat transfer characteristics are presented for a wide range of gap ratios ($1 \leq L/D \leq 8$) between two cylinders, where L and D are the distance between the cylinders and the cylinder diameter, respectively. Following successful validation, the study is extended to the flow past tandem circumferentially grooved heated cylinders. It is shown that texturing the surfaces of both cylinders reduces heat transfer compared with tandem smooth cylinders, while texturing with circumferentially grooved surfaces increases the drag coefficients of the upstream and downstream cylinders. Regardless of the Reynolds number, the critical gap ratio for the grooved cylinders in tandem is $L/D = 4$ since the Nusselt number becomes minimum at this gap ratio, while both the drag coefficient and the Strouhal number become independent of the gap ratio after that.

Keywords. Tandem cylinders; grooved surfaces; computational fluid dynamics; heat transfer.

1. Introduction

Over the years, significant research has been dedicated for understanding fluid flow around cylinders with different cross-sectional shapes, particularly circular, elliptical, square, and rectangular, because such flows are encountered in many applications, such as heat exchangers, pier legs, submarines, and offshore structures, electronic components, etc. Although the flow past smooth cylinders has been the main subject of several studies, the hydrodynamic and heat transfer characteristics of flow over modified cylinders are relatively new. In the case of modified (or textured) cylinders, the cylinders are covered with wires, riblets, or grooves circumferentially or longitudinally. Studies on tandem grooved cylinders are quite rare, even though there are practical applications such as tandem water storage tanks and twin towers [1].

When a circular cylinder is circumferentially covered with riblets or grooves along its span, the flow becomes two-dimensional (2D), reducing computational effort and time [2]. Modifications to the cylinders are generally done to increase heat transfer and reduce drag force, because it is known that roughness changes the surface conditions of a structure and its hydrodynamic properties. The early studies of turbulent flow over flat plates covered with V-type riblets showed that it is possible to reduce drag by 8% when the smaller eddies are larger than the riblet spacing, and only a limited area of the riblets is exposed to momentum exchange [3]. However, it was later shown that the drag might increase if the recirculation regions inside the grooves remain in the groove valleys, interact with the groove walls, and thereby increase viscous dissipation and drag. In this context, several studies have been performed for cylinders covered with riblets or grooves [4, 5]. A numerical study for flow over a cylinder covered with 24 cavities shows that the drag coefficient (C_d) can be reduced by 18–46% for the Reynolds number $20 \leq Re \leq 300$ in comparison with the smooth one [6]. Similarly, it was later experimentally verified that wall-pressure fluctuations on a cactus-analogue cylinder can be reduced by up to 50% at most stations [7]. A rotating grooved cylinder with varying depths shows that C_d increases with rotational speed for $Re > 10^5$ [8]. For a fixed circular cylinder, as the roughness increases, the critical point shifts to a lower Reynolds number, and C_d of a rough cylinder becomes smaller than that of the smooth cylinder. However, for rough cylinders,

Published online: 29 July 2026

as the Reynolds number (Re) increases further, C_d increases. It was reported that for a grooved cylinder with rectangular roughness, the critical Reynolds number is smaller than that for a circular cylinder without grooves [9, 10]. The flow around a smooth cylinder and a longitudinally grooved cylinder was investigated experimentally for $74{,}000 \leq \mathrm{Re} \leq 18{,}000$ [11]. It was claimed that U-shaped grooves are more effective at reducing drag than V-shaped grooves. A common feature is that these grooves are typically small-scale, with the groove depth-to-cylinder diameter ratio less than 3% [4]. As an important parameter for flow over grooved cylinders, the groove height was investigated over a wide range of Re [12], and it was found that the effect of groove height is similar to that of Re on the smooth cylinder. A comparison made between smooth and grooved cylinders, where the grooved cylinder was obtained by only one triangular-shaped cavity, shows that the groove causes a higher C_d than the cylinder without any groove. Utilizing particle image velocimetry (PIV), Caliskan *et al* [13] investigated the flow past smooth and grooved cylinders separately, where the grooved one was obtained by only one triangular-shaped cavity. The location of the groove relative to the freestream, as the cylinder was rotated at different angles, and the gap between the cylinder and the bottom wall were investigated. It was reported that the groove results in a higher C_d than that of the cylinder without a groove. Employing large eddy simulation (LES) to investigate the flow over a circular cylinder covered with circumferential and longitudinal triangular riblets demonstrated that the flows on the two sides of each riblet interact, forming a structure with stronger turbulent fluctuations and a shorter recirculation length than on bare cylinders [2]. The wake interaction between two tandem cylinders has been thoroughly investigated in the related literature; however, not as much as the flow past a single cylinder. Aiming to close the gap, Carmo and Meneghini [14] investigated small-scale instabilities of vortex shedding that occur at $160 \leq \mathrm{Re} \leq 320$ for flow past tandem smooth cylinders for $1.5 < L/D < 8.0$, where L and D are the length between the cylinders and diameter, respectively. Two smooth circular cylinders in tandem for both laminar and turbulent flows were studied in [15]. The influence of the gap ratio on the flow characteristics was taken into account for $1.5 \leq L/D \leq 5.5$. For a fixed gap ratio ($L/D = 4$), three distinct flows for laminar flow past two tandem cylinders as Re changes were identified [16] and called the reattachment flow ($50 \leq \mathrm{Re} \leq 75$), transition flow ($75 < \mathrm{Re} < 100$), and co-shedding flow ($100 \leq \mathrm{Re} \leq 200$). It was reported that the two-cylinder flow is more sensitive to Re than the single-cylinder flow, and that the tandem-cylinder flow regimes depend on the spacing between the cylinders and Re.

The advancement in the numerical methods and computing tools enable researchers to investigate the flow past smooth cylinders in tandem [17–30] at relatively low Re by means of computational fluid dynamic (CFD) method where results were presented in terms of the power spectrum density, velocity and vorticity fields, streamlines and some important non-dimensional numbers such as the Nusselt and the Strouhal numbers and the lift, drag and pressure coefficients. CFD was also used to study the influence of surface texture on these parameters for single cylinders [31–45], where several texture types, including U, V, rectangular, and triangular grooves, were employed.

Upon reviewing the literature, it is seen that numerous studies have explored the flow past cylinders in tandem. However, these studies predominantly focused on smooth-surfaced cylinders. Notably, for flow past a single cylinder or tandem cylinders, only single-groove configurations were considered. It is clear that there is a significant gap in the literature regarding flow and heat transfer studies of circumferentially fully grooved cylinders in a tandem arrangement, and this study aims to close this gap across a wide range of gap ratios and Re.

2. Computational model

In the present study, a 2D, unsteady turbulent flow of an incompressible Newtonian fluid (air) with a uniform inlet velocity across tandem cylinders with two different surface configurations, smooth and grooved, was taken into account. The present chapter introduces the dimension of the computational domain, grid structure, sensitivity, and governing mathematical equations.

2.1 *Computational domain*

Two identical circular cylinders, arranged in tandem, were placed between two parallel walls (figure 1). The origin of the Cartesian coordinate system was located at the center of the first cylinder. The computational domain covers the area $-15 < x/D < 25$ in the stream-wise direction and $-15 < y/D < 15$ in the normal direction. The uniform velocity inlet was specified at the inlet of the domain, which was $15D$ upstream of the first cylinder. The outlet placed $25D$ away from the first cylinder was assumed to be a pressure outlet, while the top and bottom surfaces of the domain were specified as walls.

The no-slip boundary condition was applied to the top and bottom walls and the cylinder surfaces. Effects of gaps

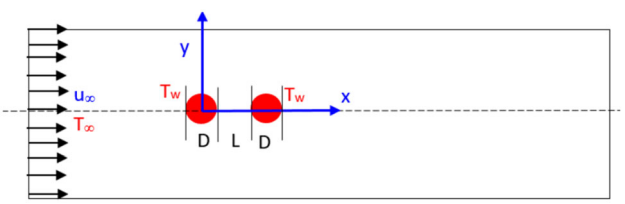

Figure 1. Computational domain.

between two identical cylinders were investigated for various dimensionless distances of $1 \leq L/D \leq 8$, where L is the gap between the surfaces of the tandem cylinders.

2.2 *Grid structure*

The structured quadrilateral cells of non-uniform grid spacing were generated to be sufficiently fine to capture the steep gradients near the cylinders (figure 2). As the distance between the cylinders increases, the grid becomes coarser to minimize computational costs while maintaining accuracy in critical regions. The grid elements are particularly fine and detailed around the periphery of the cylinders, ensuring that the boundary layer and near-wall flow phenomena are accurately captured.

2.2.1 *Grid sensitivity study.* A grid sensitivity study for a smooth cylinder was conducted using five grid sets to determine the optimal grid number. The thickness of the first grid near the wall of the cylinder was set as $0.00415D$, corresponding to non-dimensional grid distance unity (y^+=1). The coarsest grid set, called G1 employs 42,000 grid elements while the finest grid set (G5) uses 195,000 elements. The other sets are placed between them and called G2–G4, as shown in table 1.

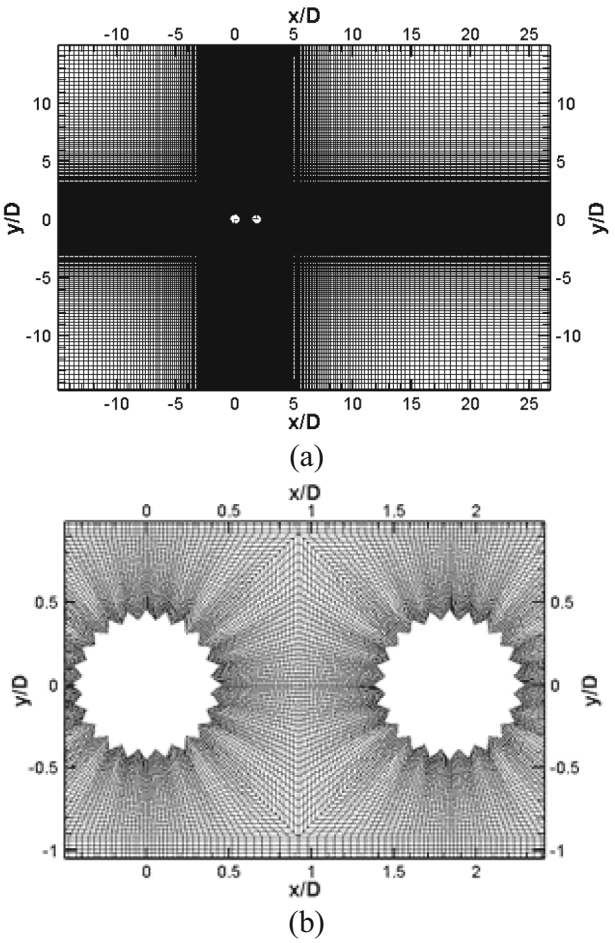

Figure 2. (**a**) Grid structure applied to the domain and (**b**) a close-up view of the grid elements around the grooved cylinders when L/D = 1.

The change in C_d concerning the number of grid elements shows that increasing the number of grid elements beyond a certain point, in this case, G3 with 118,000 elements, does not significantly affect C_d and hence, G3 was used for the remaining simulations for both smooth and grooved tandem cylinders.

2.2.2 *Time-step sensitivity study.* A time-step independence test was conducted because it affects the accuracy and stability of unsteady simulations. Four time steps, ranging from 0.0008 to 0.07 s, were tested to determine the optimal time step. As shown in table 2, the difference relative to the experimentally found C_d [46] decreases, and the smaller difference is observed for the largest time step (Δt = 0.07 s), which implies that the larger time steps yield more accurate C_d values. Therefore, this time step was used during the unsteady simulations.

The calculations were stopped when the lift (C_L) and drag coefficients (C_d) became fully periodic. Figure 3 displays a comparison of C_d over flow time for two circular smooth cylinders in tandem. The drag coefficient of the second cylinder $(C_d)_2$ shows less variability and appears to have reached a more stable state than C_d of the first cylinder $(C_d)_1$. High frequency and amplitude of oscillations of the first cylinder suggest that the flow over the first cylinder is unstable with respect to the second one. The smoother, more regular oscillations of flow over the second cylinder suggest a more controlled, stable flow. Similarly, the lift coefficient of the second cylinder $(C_L)_2$ exhibits larger, more irregular fluctuations than the first cylinder, indicating strong interactions between the cylinders. The presence of both high-frequency small-amplitude and low-frequency large-amplitude oscillations suggests complex flow behavior due to vortex shedding. Figure 4 presents the power spectrum density (PSD) as a function of the Strouhal (St) number for a smooth cylinder. The plot shows a single sharp peak in PSD centered at $St \cong 0.315$. Since St describes oscillating flow mechanisms, particularly vortex shedding, the sharp peak indicates a dominant frequency in the signal, corresponding to vortex shedding from the cylinder. It is noted that the lift coefficient was used to calculate St, which is shown here.

2.3 *Governing equations*

The governing equations of 2D, incompressible, Newtonian, and unsteady turbulent flow are the continuity and momentum equations, as shown in eqs. (1) and (2), respectively.

$$\nabla \cdot u = 0, \tag{1}$$

Table 1. Grid sensitivity study (smooth cylinder, Re = 65,000).

Title	Grid			C_d	Change in C_d (%)
	Type	Number	Change (%)		
G1	Quadrilateral	42,000	–	1.2	–
G2		94,500	125	1.2	–
G3		118,000	24	1.15	4
G4		150,000	27	1.15	–
G5		195,000	30	1.15	–

Table 2. Time-step sensitivity study (smooth cylinder, Re = 65,000).

Time step, Δt (s)	$(C_d)_{CFD}$	$(C_d)_{Exp,}$ [46]	Difference (%)
0.0008	1.45	1.08	34
0.0035	1.41		30
0.03	1.28		18
0.07	1.15		6

$$\frac{\partial u}{\partial t} + (u \cdot \nabla)u = \frac{1}{\rho}\nabla P + v\nabla^2 u, \tag{2}$$

where ∇ is the Del operator, u, P, and v are the velocity vector, pressure, and kinematic viscosity of the fluid. When the velocity is considered as the mean and fluctuating components according to Reynolds averaging, the momentum equation is called the Reynolds-averaged Navier–Stokes (RANS) equation, which contains some additional terms called Reynolds (turbulent) stresses. For the sake of the closing process, some new equations, called turbulence models, are used. In the present study, the delayed detached eddy simulation (DDES) coupled with the shear stress transport (SST) k-omega turbulence model was used. The detached eddy simulation (DES) models, often referred to as hybrid LES-RANS models, combine RANS and LES for applications such as high-Reynolds-number external aerodynamic simulations. The solution field in a DES comprises its RANS region, where a RANS turbulence model is active, and its LES region, where a LES treatment is applied [17]. The computational costs of the DES are lower than those of LES but higher than those of RANS solutions. The difference with the LES model is that it relies only on the required resolution in the boundary layers. In the DES approach, the unsteady RANS models are employed in the boundary layer. In the core turbulent region, the DES models recover LES-like sub-grid models. In the near-wall region, the respective RANS models are recovered. The standard RANS models use the distance to the closest wall, d, as a length scale while the DES uses a new length scale ($\widetilde{d}$) everywhere in the equation [47].

$$\widetilde{d} = \min(d, C_{DES}\Delta), \tag{3}$$

where $C_{DES} = 0.61$ is a constant and Δ is the grid spacing, based on the largest dimension of the grid cell:

$$\Delta = \max(\Delta x, \Delta y, \Delta z). \tag{4}$$

DDES eliminates the possibility of the modeled stress depletion (or grid-induced separation), which the original DES may suffer. The governing equations of the SST k-ω-based DDES method to simulate the unsteady flow over the cylinders are given in eqs. (5) and (6), [48].

$$\frac{\partial(\rho k)}{\partial t} + \frac{\partial(\rho k u_i)}{\partial x_i} = \frac{\partial}{\partial x_j}\left[(\mu + \sigma_k \mu_t)\frac{\partial k}{\partial x_j}\right] + P_k - \frac{\rho\sqrt{k^3}}{l_{DDES}}, \tag{5}$$

$$\frac{\partial(\rho\omega)}{\partial t} + \frac{\partial(\rho\omega u_i)}{\partial x_i} = \frac{\partial}{\partial x_j}\left[(\mu + \sigma_\omega \mu_t)\frac{\partial \omega}{\partial x_j}\right] + 2(1 - F_1)\frac{\rho\sigma_{\omega 2}}{\omega}\frac{\partial k}{\partial x_j}\frac{\partial \omega}{\partial x_j} - \rho\omega^2\beta + \frac{\rho\alpha}{\mu_t}P_k, \tag{6}$$

where turbulence viscosity (μ_t), blending functions of the SST k-ω (F_1 and F_2) are defined as in eqs. (7)–(14), respectively.

$$\mu_t = \frac{\rho k \alpha_1}{\max(\omega\alpha_1, SF_2)}, \tag{7}$$

$$F_1 = \tanh\left(arg_1^4\right), \tag{8}$$

$$arg_1 = \min\left[\max\left(\frac{\sqrt{k}}{C_\mu \omega d_\omega}, \frac{500\nu}{\omega d_\omega^2}\right), \frac{4\rho\sigma_{\omega 2}k}{CD_{k\omega}d_\omega^2}\right], \tag{9}$$

$$P_k = \min\left(\mu_t s^2, 10C_\mu\rho k\omega\right), \tag{10}$$

$$l_{DDES} = l_{RANS} - f_d \max(0, l_{RANS} - l_{LES}), \tag{11}$$

$$l_{LES} = C_{DES}H_{max}, \tag{12}$$

$$l_{RANS} = \frac{\sqrt{k}}{C_\mu \omega}, \tag{13}$$

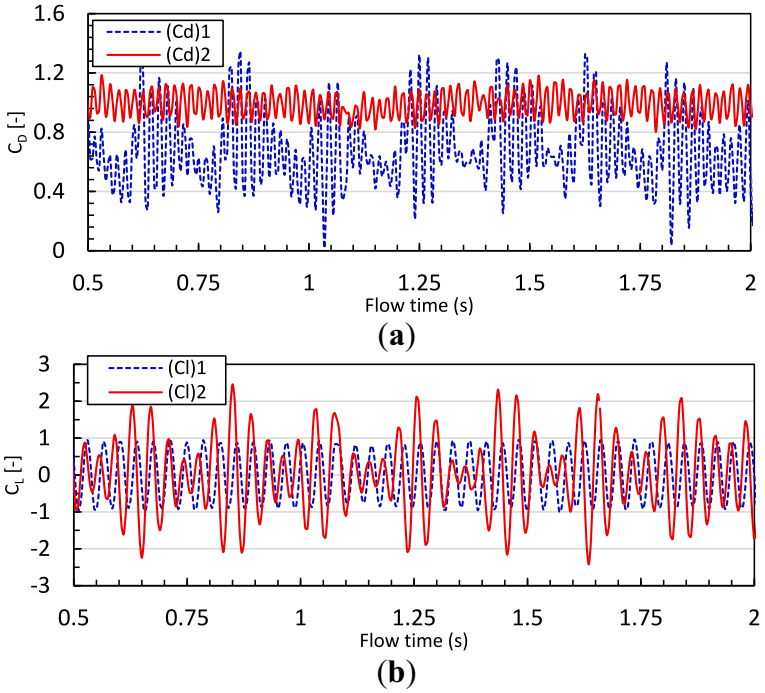

Figure 3. (**a**) C_{d} and (**b**) C_{L} variations of smooth cylinders when L/D = 6, Re = 65,000.

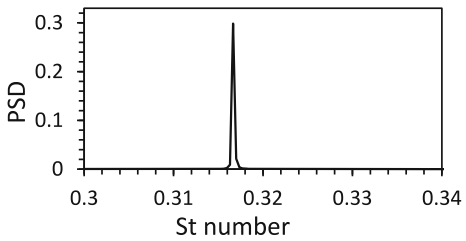

Figure 4. Strouhal (St) number (smooth cylinder, L/D = 5, Re = 65,000).

$$C_{\mathrm{DES}} = F_1 C_{\mathrm{DES1}} + (1 - F_1) C_{\mathrm{DES2}}, \tag{14}$$

where $H_{\max}$ is the maximum edge length of the local grid. The empiric blending function f_d is given in eqs. (15) and (16).

$$f_d = 1 - \tanh\left[\left(C_{d1} r_d\right)^{C_{d2}}\right], \tag{15}$$

$$r_d = \frac{v_t + v}{k^2 d_w^2 \sqrt{0.5\left(s^2 + \Omega^2\right)}} \tag{16}$$

where s is the strain rate tensor and Ω is the vorticity tensor. For flow past cylinders, some of the most important non-dimensional numbers are C_{d}, C_{L}, and St (eq. (17)). Note that C_{L} was then used to calculate the St.

$$C_{\mathrm{d}} = \frac{F_{\mathrm{D}}}{0.5\rho A u_\infty^2},\ C_{\mathrm{L}} = \frac{F_{\mathrm{L}}}{0.5\rho A u_\infty^2},\ \mathrm{St} = \frac{f_{\mathrm{D}}}{u_\infty}, \tag{17}$$

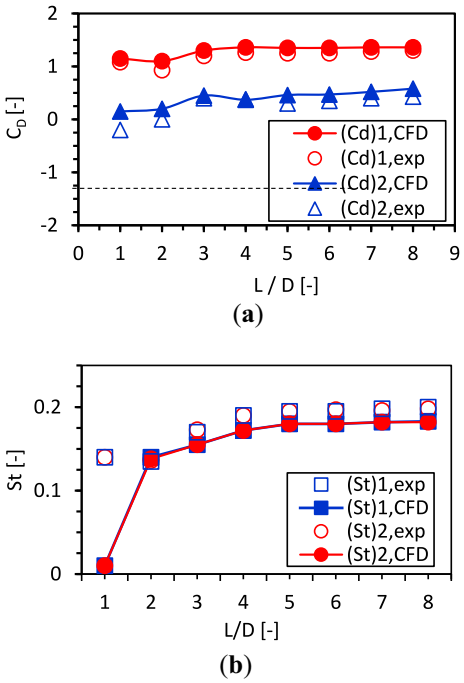

Figure 5. Comparison of the present study with the experimental data [46]. (**a**) C_{d} and (**b**) St for smooth tandem cylinders (Re = 65,000).

where F_{D}, F_{L}, ρ, A, and f stand for drag and lift forces, density of the fluid, area of the cylinder normal to the direction of forces, and frequency, respectively. The

Table 3. Comparison of Nu for tandem smooth cylinders (Re = 10, Pr = 1, *L*/*D* = 4).

	Nu_1			Nu_2	
	Num. [49]	Present study	Hilpert correlation	Num. [49]	Present study
	2.26	2.11	2.21	1.55	1.25
Difference (%)	6.6		4.5	19	

Table 4. Comparison of Nusselt numbers for grooved cylinders, Re = 10, Pr = 1, *L*/*D* = 4.

Present study	Nu_1	Nu_2
Smooth cylinders	2.11	1.25
Grooved cylinders	1.39	0.79
Change (%)	35	36

bounded central differencing scheme was used to discretize the convective terms in the momentum equation. The SIMPLE scheme was used for solving the pressure–velocity decoupling. The convergence criterion of 10^{-5} was used for the residuals of continuity, *x*- and *y*-momentum equations. The 2D, unsteady, turbulent, segregated solver was used in Ansys Fluent.

3. Results and discussion

3.1 *Validation*

Before analyzing the turbulent flow over the grooved cylinders, the present numerical study is validated using tandem smooth cylinders.

Two cases from the literature were selected for validation. The first comparison involved unheated smooth tandem cylinders as studied experimentally [46]. Figure 5(a) shows that while $(C_d)_1$ was accurately captured, $(C_d)_2$ shows discrepancies. The study struggled to predict the drag coefficient of the second cylinder at the smaller gaps (*L*/*D* = 1 and 2), likely due to the complex flow between closely spaced cylinders. However, as the gap increases, the flow stabilizes, and the model more accurately predicts the drag of both cylinders as reported in [49].

Figure 5(b) presents St derived from the spectral analysis of the fluctuating lift force on the cylinders. Similar to C_d, the St number is not accurately predicted at the smallest gap (*L*/*D* = 1), but the predictions improve at larger distances.

The second comparison was made for heated smooth tandem cylinders in a cold environment, as used in [50]. The present computational model was also compared with the Hilpert correlation reported in the literature, $Nu_D = 0.911(Re_D)^{0.385}$, for the first cylinder. As shown in table 3, the predicted Nusselt number (Nu) for the first cylinder is acceptable compared with the Hilpert correlation and the value reported by [50]. However, the numerically calculated Nu is under-predicted. A relatively large difference in Nu for the second cylinder is detected since the second cylinder lies in the unsteady wake region of the upstream cylinder, which makes its heat transfer more sensitive to small changes in gap and the flow type, such as the reattachment and shedding, as reported in multiple studies [51–53]. In both studies, Nu_2 typically shows a higher deviation than Nu_1.

3.2 *Heat transfer*

To determine the effect of surface texture on heat transfer, the Nu of both smooth and grooved cylinders were compared (table 4). In both cases, the upstream cylinder typically has a higher Nu due to its direct exposure to the flow, while the downstream cylinder experiences the wake effects of the upstream cylinder, leading to lower heat transfer rates. This effect is exacerbated by grooves since the introduction of grooves on the cylinders has led to a substantial decrease, by 35% and 36%, respectively, in the Nu in comparison with the smooth cylinders.

The decrease in Nu when the cylinders are textured with grooves indicates that the grooves disrupt the flow patterns and, accordingly, reduce convective heat transfer, even though the surface area is increased. In fact, some studies [54, 55] reported that grooves/roughness enhance heat transfer by promoting turbulence and increasing surface area; however, the effectiveness of this approach depends strongly on the specific flow conditions and Re. In certain configurations and flow regimes, grooves can have the opposite effect, especially if they cause excessive flow separation or disrupt the flow patterns required for effective convective heat transfer [56]. The flow and temperature fields shown in figure 6 indicate that reduced heat transfer occurs from grooved cylinders because the grooves promote early flow separation, leading to chaotic flow that disrupts efficient heat transfer from the cylinder surface to the surrounding fluid.

It is also observed that the grooves cause a thicker boundary layer to develop on the cylinder surface, acting as an insulating layer that reduces the temperature gradient

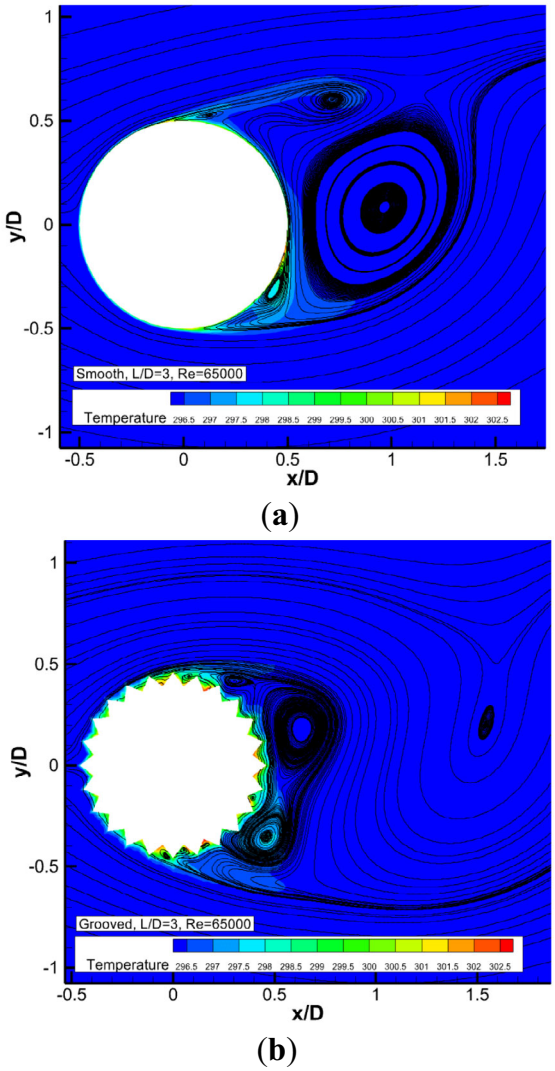

Figure 6. Temperature contours and streamlines around the (**a**) smooth and (**b**) grooved cylinder when L/D = 3, Re = 65,000.

between the cylinder surface and the fluid, thereby decreasing the heat transfer rate. Additionally, the grooves create longer conductive paths within the cylinder material, potentially increasing thermal resistance. As a result, the combined effects of altered flow separation, thicker boundary layers, and disturbed wake interference in the tandem arrangement result in lower heat transfer than that from smooth cylinders.

Heat transfer performance for smooth and grooved cylinders with various gap ratios is shown in figure 7, which shows that, regardless of surface texture, the first cylinder always provides higher heat transfer than the second one, except at L/D = 1.

However, it was noted before that due to complex flow at this gap ratio, the model developed in the present study is incapable of predicting the flow properties at L/D = 1. Therefore, it can be disregarded. The Nu for the upstream

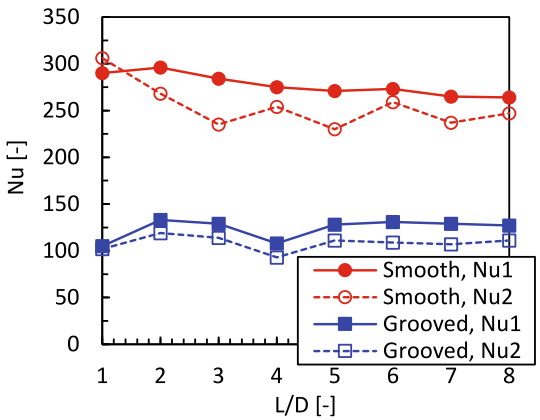

Figure 7. Comparison of Nu for smooth and grooved tandem cylinders at Re = 65,000.

and downstream smooth cylinders are consistently higher than those for grooved cylinders at all gap ratios. The Nu of the first smooth cylinder (Nu_1) decreases slightly by increasing the gap between the cylinders, while for the grooved cylinders, the Nu reduces up to L/D = 4 and then increases to its maximum at L/D = 5. Then, the Nu becomes almost constant and independent of the higher gap ratios. For the grooved cylinders in tandem, L/D = 4 is the gap that makes Nu minimum.

Several experimental and numerical studies were devoted to the critical gap between tandem cylinders. For a wide range of Re ($50 \leq Re \leq 2.5\times10^5$), the critical gap is defined as the dimensionless spacing (L/D) between identical circular tandem cylinders at which several key flow characteristics such as the flow pattern between the cylinders, St in the wake, both C_L and C_d on the cylinders change abruptly [57]. The present study reveals that Nu can be added to these parameters, as it changes abruptly at L/D = 4.

Yang and Stremler [58] summarized such past studies for Re = 100 where the critical gap or spacing (l_c) was in the range of $1.5 < l_c < 5.6$. For square cylinders in tandem, the critical gap is found as L/D = 4 at Re = 65,000 since the pressure distribution and aerodynamic forces on both cylinders change [59].

Figure 8 presents the variation in Nu with various spacing ratios and Re for tandem grooved cylinders. The Nu increases with Re, indicating enhanced convective heat transfer at higher flow rates as reported in [60, 61]. For all values of Re, the Nu of the upstream grooved cylinder is consistently higher than that of the downstream grooved cylinder. The trend of higher Nu_1 compared to Nu_2 indicates the shielding effect of the upstream cylinder on the downstream cylinder in the tandem arrangement. The peak Nu occurs around L/D = 2 for all values of Re, suggesting optimal spacing for heat transfer efficiency.

That is also the case for the smooth cylinders, as shown before. The reason is that at smaller gap ratios, the flow is

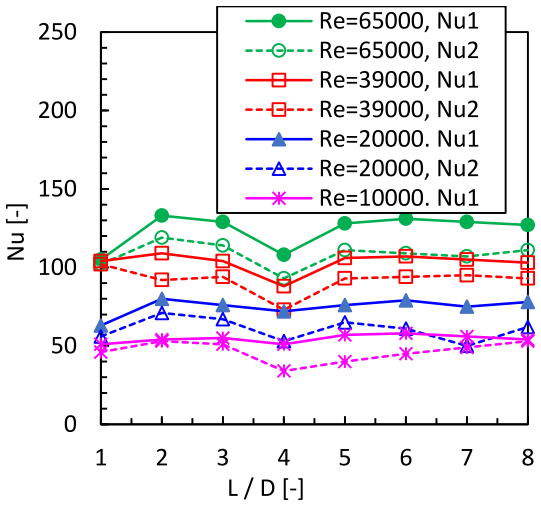

Figure 8. Distribution of Nu and Re with spacing ratios between grooved tandem cylinders.

more constricted, leading to higher fluid velocity near the cylinder surfaces. This higher velocity enhances heat transfer by promoting better mixing and sweeping away the hot layer around the cylinders, resulting in a higher Nu at a specific Re.

3.3 *Drag coefficient and Strouhal number*

The effects of both the spacing ratio and surface texture on the drag coefficient of cylinders in a tandem arrangement are presented in figure 9. Regardless of the distance between the cylinders, both the upstream and downstream grooved cylinders have higher drag coefficients than the smooth cylinders, due to the increase in surface area at $L/D = 1$. After that, both grooved and smooth cylinders exhibit similar trends, with stable C_d as the gap ratio increases.

For the downstream grooved cylinder, a negative drag coefficient is obtained at $L/D = 1$. The reason is the suction effect caused by the close proximity of the two textured cylinders. However, this effect diminishes as the gap ratio increases and the drag coefficient for the downstream cylinder stabilizes, suggesting reduced interaction between the wakes of the two textured cylinders. Furthermore, the plots reveal that the drag coefficient for all cylinders follows a similar trend, that is, as the gap ratio increases up to $L/D = 4$, the drag coefficient oscillates by increasing and decreasing, but after $L/D = 4$ it remains almost constant and becomes independent of the gap ratio. As seen in figure 9(b), both the smooth and grooved upstream and downstream cylinders exhibit a similar trend with the spacing ratio: St increases with increasing L/D until $L/D = 4$, after which it stabilizes. Considering the change in C_d that is stabilized for both upstream and downstream cylinders and the St at $L/D = 4$, it can be concluded that

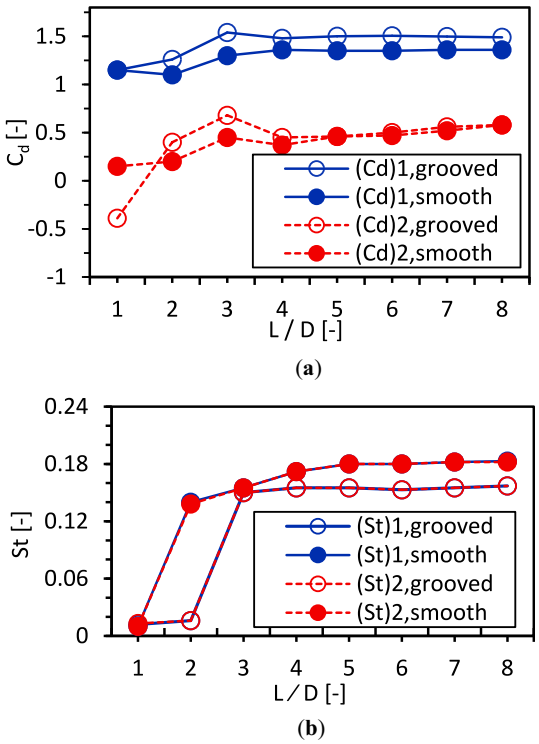

Figure 9. **(a)** C_d and **(b)** St of the smooth and grooved cylinders in tandem arrangement, Re = 65,000.

$L/D = 4$ is a critical distance, as significant changes in flow dynamics occur at that spacing ratio. Beyond $L/D = 4$, the St make a plateau, revealing that the distance between the cylinders beyond this gap ratio has a lesser impact on oscillation frequencies. In terms of surface texture, the St of grooved and smooth cylinders differs slightly once the gap ratio exceeds 4. Stabilization of St suggests a transition to a steady wake-interference pattern between the cylinders, reducing the influence of further increases in the gap ratio.

3.4 *Flow and temperature fields*

Figure 10 displays the temperature contours and streamlines between tandem grooved cylinders for the gap ratios $1 \leq L/D \leq 8$. This figure displays the impact of different spacing ratios on the temperature distribution and flow patterns. In the first gap ratio, where the cylinders are the closest to each other, a strong interaction between their wakes occurs. The flow exhibits significant recirculation zones behind the upstream cylinder, which affect the flow around the downstream cylinder. The temperature field shows a narrow wake with high-temperature gradients due to the proximity, leading to limited mixing. Increasing the gap to $L/D = 2$ allows more space for the wake to develop between the cylinders. The flow shows well-defined vortex shedding from both cylinders, with interaction still present but less intense than the previous gap ratio. The contours

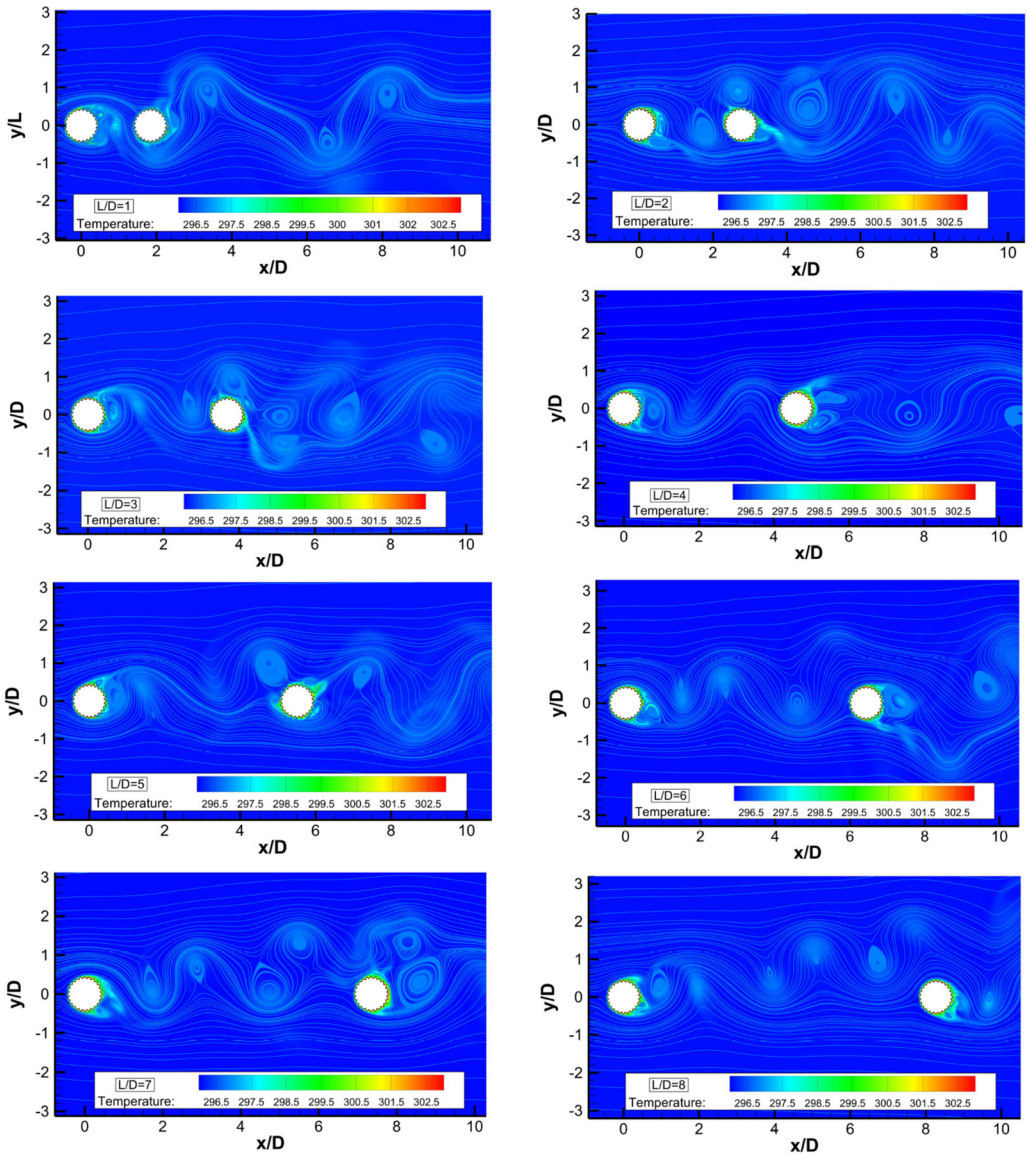

Figure 10. Temperature contours and streamlines between the tandem grooved cylinders for $1 \leq L/D \leq 8$, Re = 10,000.

indicate more pronounced thermal mixing and spreading downstream. In the third case, where $L/D = 3$, the wake structures become more distinct, with clearer separation between the vortices from each cylinder. Flow interaction is moderate, with the upstream cylinder's wake influencing the downstream one but allowing for more developed flow patterns. The temperature field shows increased mixing, with a wider spread of the thermal contours downstream. For $L/D = 4$, the wake interaction decreases further, with each cylinder producing its own distinct wake that eventually merges. Flow patterns show alternating vortices with less direct interference from the neighboring cylinder's wake. The temperature distribution becomes more uniform, indicating efficient mixing. With $L/D = 5$, the wakes of the cylinders are more independent, showing reduced interaction. The streamlines depict periodic vortex shedding with minimal direct influence between the wakes. The temperature contours continue to show good mixing, with the thermal field spreading evenly downstream. At $L/D = 6$, the cylinders are sufficiently spaced apart that their wakes develop independently before merging downstream. Flow exhibits clear, periodic vortex shedding with well-separated vortical structures. The temperature distribution remains uniform, with efficient thermal mixing extending further downstream. As the gap ratio increases further, the wakes are almost completely independent, with each cylinder's wake developing without significant interference from the other. The flow patterns show consistent, periodic vortex

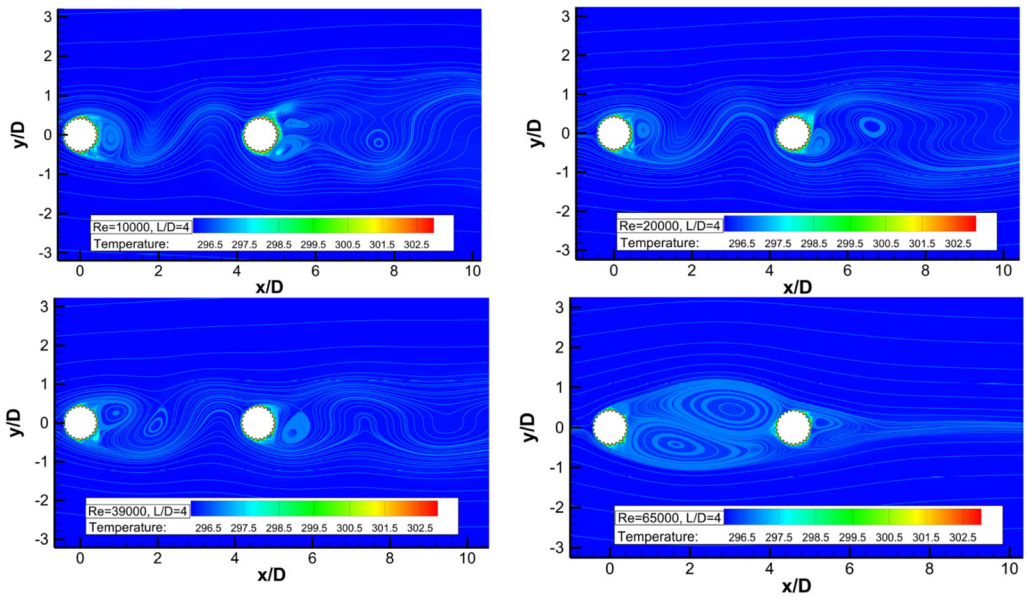

Figure 11. Effects of Reynolds number on the temperature and flow fields between tandem grooved cylinders, $L/D = 4$.

shedding with distinct vortices. The temperature field indicates good mixing, with the thermal contours spreading widely downstream.

Figure 11 displays the effects of Re on the temperature and flow fields between tandem grooved cylinders with a fixed spacing ratio of $L/D = 4$. This gap ratio was selected because it is the critical gap ratio. At the lowest Re, the flow exhibits well-defined vortices forming behind each cylinder. The wake region is characterized by significant temperature variations, as indicated by the contours, which show the spread and interaction of thermal effects. The temperature field downstream of the upstream cylinder influences the upstream flow of the downstream cylinder, leading to a complex temperature distribution between the cylinders. For Re = 20,000, the wake behind the cylinders becomes more pronounced and elongated. The vortices are more separated compared to Re = 10,000, indicating stronger and more distinct shedding. There is an observable increase in the temperature variation within the wake regions, suggesting enhanced mixing and heat transfer. At Re = 39,000, the wake structures become more intricate, showing more turbulent behavior. The vortex shedding appears more regular and periodic, with clear alternating patterns of high- and low-temperature regions downstream. The interaction between the wakes of the two cylinders leads to a more complex temperature distribution, with noticeable variations in the thermal field. At the highest Re, the flow exhibits strong turbulence. The wake regions are highly disturbed, with smaller and more numerous vortical structures. The temperature contours show significant spreading and mixing, indicating very efficient heat transfer due to the increased turbulence.

4. Conclusion

This numerical study presents the results of heat transfer and flow past two tandem circumferentially grooved circular cylinders for various Re and gap ratios, using the DDES method. It is observed that regardless of the cylinders' surface texture, as the gap ratio increases, the interaction between the wakes of the cylinders decreases. When the cylinders are close to each other, the wakes interact strongly, leading to complex flow patterns and temperature distributions. As the spacing increases, the interaction weakens, resulting in more distinct and regular vortex shedding patterns. The flow transitions from highly interactive and complex at lower gap ratios to more independent, regular vortex shedding at higher gap ratios. This progression highlights the diminishing influence of the upstream cylinder on the downstream flow as the gap increases. The temperature contours indicate that thermal mixing improves with increasing gap ratio. At lower gaps, the temperature field is more constrained with higher gradients. As the spacing increases, the temperature distribution becomes more uniform, indicating efficient mixing and downstream spreading of thermal effects. Comparisons of the drag coefficients and St indicate that the present study can predict these parameters for both the first and second cylinders, except at the smallest gap ratio. In the case of

surface texture, such as being smooth or grooved, the study reveals that while grooves have some advantages, such as affecting drag coefficients or vortex shedding frequencies, it negatively impacts the convective heat transfer capability of the cylinders in this configuration. The flow regime characterized by Re has a significant impact on heat transfer between tandem grooved cylinders. Higher Re promotes better mixing and a more uniform temperature distribution.

References

[1] Derakhshandeh J F, Gharbia Y and Ji C 2022 Numerical investigations on flow over tandem grooved cylinders. *Ocean Eng.* 251: 111160

[2] Xing F and Lei C 2022 A large eddy simulation of flow over a circular cylinder with circumferential triangular riblets: Effects of spanwise coverage ratio. *Ocean Eng.* 263: 112439

[3] Walsh M J 1982 Turbulent boundary layer drag reduction using riblets. *AIAA Aerospace Sciences Meeting*, pp. 11–14

[4] Lim H C and Lee S J 2003 PIV measurements of near wake behind a U-grooved cylinder. *J Fluid Struct* 18: 119–130

[5] Alonzo-García A, Gutiérrez-Torres C D C, Jiménez-Bernal J A, López-Aguado-Montes J L, Barbosa-Saldaña J G, Mollinedo-Ponce-de-Leon H R and Martinez-Delgadillo S A 2015 Large eddy simulation of the subcritical flow over a V grooved circular cylinder. *Nucl. Eng. Des.* 291: 35–46

[6] Liu Y Z, Shi L L and Yu J 2011 TR-PIV measurement of the wake behind a grooved cylinder at low Reynolds number. *J. Fluid Struct*. 27: 394–407

[7] Wang S F, Liu Y Z and Zhang Q S 2014 Measurement of flow around a cactus-analogue grooved cylinder at $Re_D = 5.4\times10^4$: Wall-pressure fluctuations and flow pattern. *J. Fluid Struct.* 50: 120–136

[8] Takayama S and Aoki K 2005 Flow characteristics around a rotating grooved circular cylinder with grooved of different depths. *J. Visual.* 8: 295–303

[9] Aoki K, Shimada T and Takayama S 2003 Flow characteristics around circular cylinder with arc grooves. In: *Proceedings 7th Asian Symposium on Visualization* 42: 8–9

[10] Diaz F, Gavaldá J, Kawall J G, Keffer J F and Giralt F 1983 Vortex shedding from a spinning cylinder. *Phys. Fluids* 26: 3454–3460

[11] Zhou B, Wang X, Guo W, Gho W M and Tan S K 2015 Control of flow past a dimpled circular cylinder. *Exp. Therm. Fluid Sci.* 69: 19–26

[12] Cheng W, Pullin D I and Samtaney R 2018 Large-eddy simulation of flow over a grooved cylinder up to transcritical Reynolds numbers. *J. Fluid Mech.* 835: 327–362

[13] Caliskan M, Tantekin A, Ozdil N F T and Akilli H 2021 Investigation of flow characteristics for triangular grooved shape cylinder at different heights in shallow water. *Ocean Eng.* 225: 108788

[14] Carmo B S and Meneghini J R 2006 Numerical investigation of the flow around two circular cylinders in tandem. *J. Fluid Struct.* 22: 979–988

[15] Dehkordi B G, Moghaddam H S and Jafari H H 2011 Numerical simulation of flow over two circular cylinders in tandem arrangement. *J. Hydrodyn.* 23: 114–126

[16.] Derakhshandeh J F and Alam M M 2020 Reynolds number effect on the flow past two tandem cylinders. *Wind Struct.* 30: 475–483

[17] Aasland T E, Pettersen B, Andersson H I and Jiang F 2022 Revisiting the reattachment regime: A closer look at tandem cylinder flow at Re = 10000. *J. Fluid Mech.* 953: A18

[18] Alam M M 2016 Lift forces induced by phase lag between the vortex sheddings from two tandem bluff bodies. *J. Fluid Struct.* 65: 217–237

[19] Alam M M, Zheng Q, Derakhshandeh J F, Rehman S, Ji C and Zafar F 2018 On forces and phase lags between vortex sheddings from three tandem cylinders. *Int. J. Heat Fluid Flow* 69: 117–135

[20] Al-Sumaily G F, Hussen H M, Chaichan M T, Dhahad H A and Thompson M C 2023 Numerical analysis of flow shedding over an obstacle at low Reynolds number. *Int. J. Heat Fluid Flow* 99: 109098

[21] Jing H, Zhang J, Han M, Li W, Zhao W and Liu Q 2024 Numerical study on the aerodynamic characteristics and flow field of two tandem tapered square cylinders with different spacing ratios. *Ocean Eng.* 295: 116875

[22] Li Y, Shi F, Xin J, Peng L and Wan L 2024 Numerical investigation of the heat transfer and flow pattern on tandem triangle-grooved cylinders. *Case Stud. Therm. Eng.* 60: 104808

[23] Lin H, Zhu C and Jiang R 2023 Research on flow around two tandem rectangular cylinders. *Ocean Eng.* 279: 114068

[24] Mahír N and Altaç Z 2008 Numerical investigation of convective heat transfer in unsteady flow past two cylinders in tandem arrangements. *Int. J. Heat Fluid Flow* 29: 1309–1318

[25] Meneghini J R, Saltara F, Siqueira C L R and Ferrari J A 2001 Numerical simulation of flow interference between two circular cylinders in tandem and side-by-side arrangements. *J. Fluid Struct.* 15: 327–350

[26] Nazvanova A, Yin G and Ong M C 2022 Numerical investigation of flow around two tandem cylinders in the upper transition Reynolds number regime using modal analysis. *J. Marine Sci. Eng.* 10: 1501

[27] Sayehvand H O, Dehkordi K and Basiri P 2017 Numerical analysis of forced convection heat transfer from two tandem circular cylinders embedded in a porous medium. *Therm. Sci.* 21: 2117–2128

[28] Skonecki G M and Buick J M 2023 Numerical study of flow around two circular cylinders in tandem, side-by-side and staggered arrangements. *Fluids* 8: 148

[29] Wang Y T, Yan Z M and Wang H M 2013 Numerical simulation of low-Reynolds number flows past two tandem cylinders of different diameters. *Water Sci. Eng.* 6: 433–445

[30] Wang Y, Cheng W, Du R, Wang S and Deng Y 2020 Numerical investigation of flow around two tandem identical trapezoidal cylinders. *Math. Probl. Eng.* 12: 1–13

[31] Alonzo-García A, Gutiérrez-Torres C del C and Jiménez-Bernal J A 2014 Large eddy simulation of the subcritical flow over a U-grooved circular cylinder. *Adv. Mech. Eng.* 6

[32] Afgan I, Kahil Y, Benhamadouche S, Ali M, Alkaabi A, Berrouk A B and Sagaut P 2023 Cross flow over two heated cylinders in tandem arrangements at subcritical Reynolds

number using large eddy simulations. *Int. J. Heat Fluid Flow* 100: 109115

[33] Afroz F and Sharif M A R 2022 Numerical study of cross-flow around a circular cylinder with differently shaped spanwise surface grooves at low Reynolds number. *Ur. J. Mech. B-Fluid* 91: 203–218

[34] Canpolat C 2015 Characteristics of flow past a circular cylinder with a rectangular groove. *Flow Meas. Instrum.* 45: 233–246

[35] Lee S J, Lim H C, Han M and Lee S S 2005 Flow control of circular cylinder with a V-grooved micro-riblet film. *Fluid Dyn. Res.* 37: 246–266

[36] Liu P, Wang D and Yan F 2022 Experimental study on the wake characteristics of the circular cylinder with the V-groove surface. *Int. J. Nav. Arch. Ocean* 14: 100449

[37] Nouri-Borujerdi A and Nakhchi M E 2017 Heat transfer enhancement in annular flow with outer grooved cylinder and rotating inner cylinder: Review and experiments. *Appl. Therm. Eng.* 120: 257–268

[38] Ozalp C, Saydam D B, Polat C, Soyler M and Hürdoğan E 2021 Heat transfer and flow structure around a heated cylinder by upstream installation of a grooved cylinder. *Exp. Therm. Fluid Sci.* 128: 110448

[39] Patel C G, Sarkar S and Saha S K 2018 Mixed convective vertically upward flow past side-by-side square cylinders at incidence. *Int. J. Heat Mass Transfer* 127: 927–947

[40] Quintavalla S J, Angilella A J and Smits A J 2013 Drag reduction on grooved cylinders in the critical Reynolds number regime. *Exp. Therm. Fluid Sci.* 48: 15–18

[41] Song X, Qi Y, Zhang M, Zhang G and Zhan W 2019 Application and optimization of drag reduction characteristics on the flow around a partial grooved cylinder by using the response surface method. *Eng. Appl. Comput. Fluid Mech.* 13: 158–176

[42] Soyler M, Ozalp C, Polat C, Saydam D B and Yavuz M M 2022 Experimental and numerical investigation of flow structure of grooved cylinder. *Ocean Eng.* 264: 112478

[43] Yahiaoui T, Ladjedel O, Imine O and Adjlout L 2016 Experimental and CFD investigations of turbulent cross-flow in staggered tube bundle equipped with grooved cylinders. *J. Braz. Soc. Mech. Sci. Eng.* 38: 163–175

[44] Zhang K, Zhu H, Cao Y and Zhou D 2023 Reynolds number effects on the bistable flows over a wavy circular cylinder. *Ocean Eng.* 271: 113776

[45] Zhou B, Wang X, Guo W, Zheng J and Tan S K 2015 Experimental measurements of the drag force and the near-wake flow patterns of a longitudinally grooved cylinder. *J. Wind Eng. Ind. Aerodyn.* 145: 30–41

[46] Alam M M, Moriya M, Takai K and Sakamoto H 2003 Fluctuating fluid forces acting on two circular cylinders in a tandem arrangement at a subcritical Reynolds number. *J. Wind Eng. Ind. Aerodyn.* 91: 139–154

[47] Travin A, Shur M, Strelets M and Spalart P 1999 Detached-eddy simulations past a circular cylinder. *Flow Turbul. Combust.* 63: 293–313

[48] Zhang N, Liu X, Gao B and Xia B 2019 DDES analysis of the unsteady wake flow and its evolution of a centrifugal pump. *Renew. Energy* 141: 570–582

[49] Menteşe A and Bayraktar S 2021 Numerical investigation of flow over tandem and side-by-side cylinders. *Seatific Eng. Res. J.* 1: 15–25

[50] Laidoudi H and Bouzit M 2017 Mixed convection heat transfer from confined tandem circular cylinders in cross-flow at low Reynolds number. *Mechanika* 23: 522–527

[51] Hsu L C and Liang C W 2021 Heat transfer in flow past two cylinders in tandem and enhancement with a slit. *Energies* 14: 308

[52] Harimi I and Saghafian M 2012 Numerical simulation of fluid flow and forced convection heat transfer from tandem circular cylinders using overset grid method. *J. Fluid Struct.* 28: 309–327

[53] Singh S V, Mitra Praneeti and Kumar P 2021 A study of flow interference and heat transfer between two-cylinders at different orientations. *J. Ocean Eng. Sci* 6: 248–256

[54] Al-Rubaiy A A A G 2018 *The effect of surface roughness and free stream turbulence on the flow and heat transfer around a circular cylinders*. Ph.D. thesis. University of Sheffield

[55] Tetsu F, Motoo F and Masanori T 1973 Influence of various surface roughness on the natural convection. *Int. J. Heat Mass Transfer* 16: 629–636

[56] Abu-Hijleh B A K 2003 Numerical simulation of forced convection heat transfer from a cylinder with high conductivity radial fins in cross-flow. *Int. J. Therm. Sci.* 42: 741–748

[57] Zhou Y and Alam M M 2016 Wake of two interacting circular cylinders: A review. *Int. J. Heat Fluid* 62 (Part B): 510–537

[58] Yang W and Stremler M A 2019 Critical spacing of stationary tandem circular cylinders at $\mathrm{Re} \approx 100$. *J. Fluid Struct.* 89: 49–60

[59] Hossain M M, Nayeem M H K and Ali M A T 2021 Numerical study of flow characteristics around rectangular cylinders in tandem. *J. Mech. Eng. Aut. Control Syst.* 2: 36–43

[60] Bayraktar S, Tekercioglu R and Dincel A T 2019 Flow field analysis of grooved surfaces. *Int. J. Environ. Sci. Technol.* 16: 5365–5368

[61] Babaee H, Perdikaris P, Chryssostomidis C and Karniadakis G E 2016 Multi-fidelity modelling of mixed convection based on experimental correlations and numerical simulations. *J. Fluid Mech.* 809: 895–917

Springer Nature or its licensor (e.g. a society or other partner) holds exclusive rights to this article under a publishing agreement with the author(s) or other rightsholder(s); author self-archiving of the accepted manuscript version of this article is solely governed by the terms of such publishing agreement and applicable law.